Quantitative assessment of STM images of Fe grown epitaxially on MgO(001) using fractal techniques

S. M. Jordan, R. Schad, D. J. L. Herrmann, J.F. Lawler, and H. van Kempen*
Research Institute for Materials, University of Nijmegen, Toernooiveld 1, NL-6525 ED Nijmegen, The Netherlands
(Received 3 June 1998; revised manuscript received 20 July 1998)

We have assessed scanning tunneling microscope images of Fe grown on MgO(001) at various temperatures using two different methods. Evaluation of the height-height variance function reported a correlation length very close to the average island radius. The area-perimeter method reported the perimeters above which non-square-law scaling of the islands begins to be somewhat lower than the average perimeters of the discrete islands. A comparison of two common methods for evaluating length-dependent roughness is made. [S0163-1829(98)00143-X]

I. INTRODUCTION

Roughness studies of growing crystals are very attractive for several reasons. First, it is the sheer beauty of fractal systems that has fascinated researchers for decades[1] and second, kinetic roughening of the growth front during thin-film deposition[2–10] is of eminent technological importance.

The films' physical properties will very much depend on the smoothness or roughness of the final growth front that will form the interface to the adjacent material or the surface that interacts with the environment. For instance, the interfaces in field-effect transistors or tunnel junctions have to be extremely flat to guarantee homogeneous oxide thicknesses, whereas the so-called giant magnetoresistance effect in magnetic multilayers is enhanced by a certain degree of interface roughness.[11–13] Also, the performance of catalytic materials relies on a huge surface area.

Proper control of the surface properties requires an understanding of the underlying growth mechanisms. This can be achieved by the detailed structure analysis of surfaces prepared under various growth conditions. However, the roughness of a surface is a more complicated concept than the widespread use of this simple term might suggest. The size of the commonly used root-mean-square (rms) roughness, for example, in most cases depends on the lateral distance over which it is measured and therefore does not provide a comprehensive description of the surface structure.

Also necessary are quantitative estimates of the surface roughness in both vertical and lateral direction. Typically this includes the vertical rms roughness σ, the lateral correlation length ξ and the Hurst parameter H, which describes the fractal dimension D of a self-affine surface via $D=3-H$. The fractal dimension is equally important as ξ since it describes the jaggedness of the surface,[14] which, in combination with ξ, is a measure for the step density which is often the important parameter.[15,16] These parameters have to be measured by techniques fulfilling certain requirements. Their structure sensitivity must range from the smallest possible length scale (the atomic scale) up to length scales exceeding ξ and need to be strictly surface or interface sensitive. For surfaces an ideal instrument is the scanning tunneling microscope[17–20] (STM) having a dynamical range of structure sensitivity over several decades, in many cases including the required length scales. For most systems studied these measurements have to be done under ultrahigh vacuum (UHV) conditions to prevent oxidation that can alter the surface structure in an unpredictable way.

As a test system we have chosen the epitaxial growth of Fe on MgO(001) at various temperatures for several reasons. First, the substrate provides an almost uniform template with up to μm wide, atomically flat terraces, which, with respect to the structure of the Fe films grown on top, can be regarded as flat. Second, the epitaxial growth of bcc Fe provides a system with a simple fourfold in-plane symmetry without inhomogeneities like grain boundaries as found in polycrystalline samples. Third, the structure parameters estimated here are of importance for the understanding of the magnetic properties of such Fe films[21] or the transport properties of Fe/Cr superlattices.[11–13]

The analysis is done by examining STM micrographs. First, the $(2+e)$-dimensional surface roughness is analyzed for its length scale dependence. For a self-affine surface the height-height variance function, where L is the lateral distance between r and r',

$$g(L)=\langle[z(r)-z(r')]^2\rangle, \tag{1}$$

should saturate for $L \gg \xi$ at

$$g(L)=2\sigma_\infty^2 \tag{2}$$

and vary with L for $L \ll \xi$ as

$$g(L)\sim L^{2H}, \tag{3}$$

with ξ and H being as defined above, and σ_∞ being the rms roughness averaged over an infinitely large image.

The function $g(L)$ is related to the height-height correlation function

$$C(L)=\sigma_\infty^2 \exp[-(L/\xi)^{2H}] \tag{4}$$

via

$$g(L)=2\sigma_\infty^2-2C(L) \tag{5}$$

yielding

$$g(L)=2\sigma_\infty^2\{1-\exp[-(L/\xi)^{2H}]\}. \quad (6)$$

The values of σ_∞ and H can be estimated from the asymptotic behavior for, respectively, large and small values of L. The correlation length ξ is then found by a one-parameter fit to $g(L)$ using Eq. (6).

Equations (4) and (6) were introduced by Sinha *et al.*,[22] and make convenient interpolation formulas. Their use is restricted to surfaces that have a Gaussian distribution of heights, which we found to be the case. For surfaces with a non-Gaussian distribution, H can be found from Eq. (3). The x intercept between the regime where $g(L)$ scales with L and the regime where it saturates then gives ξ.

Second, the $(1+\epsilon)$-dimensional perimeter of the Fe growth structures is analyzed using the area-perimeter method.[1] A collection of similar, nonfractal islands will display a ratio[23]

$$\rho=(\text{perimeter})/(\text{area})^{1/2}, \quad (7)$$

both independent of the island's size and the resolution δ to which the dimensions are measured. This ratio ρ will be $2\sqrt{\pi}$ in the case of round islands and 4 in the case of squares.

It has been found that for islands displaying fractal properties the value of ρ measured depends on δ. As δ, the ''yardstick length'' decreases, the measured perimeter increases without limit. The scaling exponent between the perimeter P and δ is found to be $(1-D')$, where D' is the two-dimensional fractal dimension and varies between 1 and 2. The relation between D and D' is not as simple as $D=D'+1$,[20] since the fractal properties in the vertical (z) direction are important for $g(L)$. The measurements to be described in Sec. IV are quite distinct from roughness analysis.

It is practically difficult to make repeated STM scans with very different resolutions; nonetheless we are able to access D' by studying the relation between the area of an island A and P. Here the scaling law is

$$P(\delta)\propto A(\delta)^{D'/2}. \quad (8)$$

Another piece of information will be provided by this relation in that the point at which D' becomes greater than unity provides a scaling length for the onset of fractal-like behavior.

In this paper, we report a detailed structure analysis of epitaxial Fe layers grown on MgO(001) including the fractal analysis in $(2+\epsilon)$ and $(1+\epsilon)$ dimensions.

II. EXPERIMENT

Commercial MgO(001) substrates were first cleaned by washing with organic solvents to remove contaminants. They were then heated to 1070 K in UHV for 1 min and then analyzed by Auger electron spectroscopy. A *KLL* C peak was seen corresponding to 6% of 1 ML. Heating the MgO to temperatures as high as 1400 K did not reduce this contamination. Atomic-force microscopy investigations showed the substrates to be of exceptional flatness; single atom high terraces of width up to 200 nm were seen.

Fe layers were grown using a Knudsen cell at a rate of 0.13 nm per min. The iron atoms were incident at angle of 15° to the sample normal, the flux being directed along the Fe[110] axis. The sample was maintained at the required temperature by electron heating of the sample holder. The layers were all 5 nm in thickness, which provides a stable and electrically conductive film.

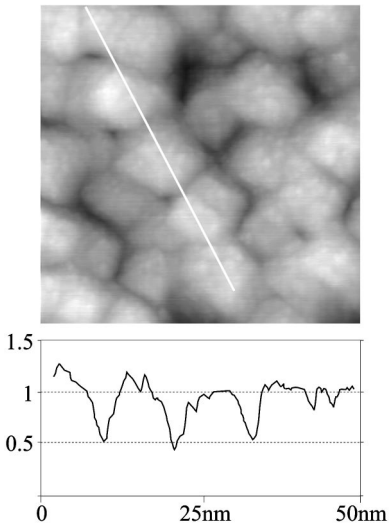

FIG. 1. STM image of 5 nm of Fe grown at 395 K, with a scan length of 50 nm. A cross section (taken along the solid line) is shown, with a height scale in nm.

The samples were then studied *in situ* by use of an in-house built STM.

III. HEIGHT-HEIGHT VARIANCE FUNCTION

We have previously reported an empirical study of the behavior of layers of bcc Fe deposited on MgO(001).[21] This STM study showed that the Fe forms round islands approximately 10 nm in diameter at growth temperatures at and below room temperature. As the deposition temperature increases, the islands become square, and increase in diameter to 30 nm. At the highest temperature we used, 595 K, just below the point at which a discontinuous film results, we were able to resolve single atomic steps of approximately $a/2$ in height.

These topographic properties of the film surfaces are a result of the underlying growth kinetics and thermodynamics. The typical island diameter is a result of the nucleation density during the start of the growth whereas the development of growth pyramids is a sign of reduced diffusion across step edges due to the so-called Schwoebel barrier.[24] The square-island shape is caused by the preference of step formation along the [100] directions, which can only be achieved when diffusion along the step edges is fast enough, thus requiring higher deposition temperatures.

A 50-nm-wide STM image for a growth temperature of 395 K is shown in Fig. 1. This illustrates the typical form and quality of our images. The height is recorded as a 16-bit digital number. A cross section of the surface, which cuts across several islands is also shown. The vertical (z) axis is not to the same scale as the horizontal axis — the steep sides of the ''valleys'' between islands make typical angles of 12° to the horizontal. Thürmer *et al.*[7] found angles of 30° on pyramid faces found in a 300-nm-thick film due to the

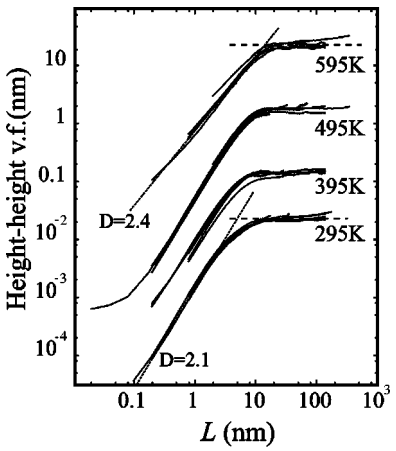

FIG. 2. The height-height variance function $g(L)$ for the four temperatures. The horizontal lines show the saturation at $2\sigma_\infty^2$. The difference in H between 495 and 595 K is clearly visible. Curves shifted vertically for clarity.

Schwoebel barrier preventing the downward diffusion of atoms at step edges; however we cannot expect this slope to have reached its final value on a film 5 nm thick.

We evaluated Eq. (1) directly. The distance L between points z and z' was varied to provide the x axis, the averaging occurring over typically 10^6 points in order to provide good statistics. The parameter L could typically be varied over four orders of magnitude; we analyzed scans of widely varying sizes to extend this range. We also removed images from the data set that showed gross and obvious defects such as large areas where contaminants are present or resolution is lost. This was the sole criterion for removing data.

No discussion of roughness measurements can be complete without a treatment of the effects of image artifacts. There are two common phenomena to take into account: the finite radius of the tip and the slope present in the image. Our data were plane-fitted (the least-squares fitted plane was removed) in both the x (fast-scan) and y directions before the division into tiles, providing an image with no overall slope. The effect of plane-fitting is discussed by Kiely and Bonnell,[18] who showed that it has a dramatic effect on $g(L)$, reducing g for lengths greater than ξ. ''Flattening,'' that is, adjusting the mean of each scan line to be the same, also reduced g for all L, but we felt that for our small scan lengths this was unnecessary, and likely to remove some of the surface structure. In this study, the images used had a scan size larger than the correlation length, as opposed to studies such as that of Krim *et al.*,[25] which used many small images that were individually plane-fitted.

The effect of tip radius has been discussed by several authors.[26,27] It is clear that it affects the measured roughness;[18] however assessing the tip radius without a reference sample is nontrivial. All images were taken with the same mechanically cut Pt-Ir tip; however, the tip's properties can change over time. *In situ* UHV use makes measurement and maintenance of a particular tip geometry difficult. It is difficult to define a radius for our tips; however they are sharp enough to resolve atomic steps and have sufficient aspect ratio to follow deep features.

Figure 2 shows the relation $g(L)$ plotted using a log-log scale. Each line in the figure is derived from a single complete scan of the surface. The small spread of the lines indicates either that our data is of high quality or that all images give very similar results. Since $g(L)$ changes in several respects when the deposition temperature is varied, we conclude that $g(L)$ measures a useful property of the image.

TABLE I. Fractal dimension (D), correlation length (see Sec. III), average island size and rms roughness averaged over a single 200-nm image summarized. The standard deviation in island sizes was approximately 15% in all cases.

Growth temp. (K)	$D\pm0.1$	ξ (nm)	Mean island radius(nm)	σ_∞ (nm)
295	2.1	4.7 ± 0.4	3.5	0.52
395	2.1	4.7 ± 0.4	4.5	0.42
495	2.1	7.9 ± 0.3	8	0.58
595	2.4	14.2 ± 1.5	15	0.28

As outlined in Sec. I, when the tile-edge length L is much greater than the size of typical features, increasing L still further does not bring higher features into a tile, and $g(L)$ saturates at $2\sigma_\infty^2$. Table I gives values of σ_∞ averaged over several *complete* 200 nm images. This number provides little information by itself, since many possible differing surfaces can give the same parameter. Examination of the surfaces leads us to conclude that the lower σ_∞ is associated with the large flat islands that appear at the highest temperature. We are confident that $g(L)$ does not increase further when $L>500$ nm.

For a temperature of 495 K, the slope of $g(L)$ begins to fall when $L<0.2$ nm. This could be due to the finite resolution of the STM, or that an image of side much less than ξ (5×5 nm) could not be plane-fitted correctly.

When L is much smaller than ξ, the scaling exponent H [Eq. (3)] can be determined. It is related to the fractal dimension by $D=3-H$. Table I gives values of D found by least squares fitting of data to the equation

$$g(L)=aL^{2H} \tag{9}$$

with $0.1<L<8$ nm. It appears that D is constant at low-deposition temperatures, but increases somewhat at 595 K.

The values of ξ were determined from the intercept of Eq. (9) and the saturation of $g(L)$ at large L using the formula

$$\xi=(2\sigma_\infty^2/a)^{1/H}, \tag{10}$$

with σ_∞ being fixed at the value presented in Table I. Average island radii along the major axes are also given; these were made by measuring the distance between the trenches on opposite sides of well-defined islands. The radii and ξ agree closely.

IV. AREA-PERIMETER RELATION

A classic method for the evaluation of D', which has been applied to such diverse systems as STM images[20] and rain cloud formation[23] is the area-perimeter method. Experimentally, the perimeters and areas of the objects to be assessed are plotted on a log-log graph and the scaling exponent determined. Mandelbrot, in Ref. 23, gives the relation between the perimeter P and the area A as

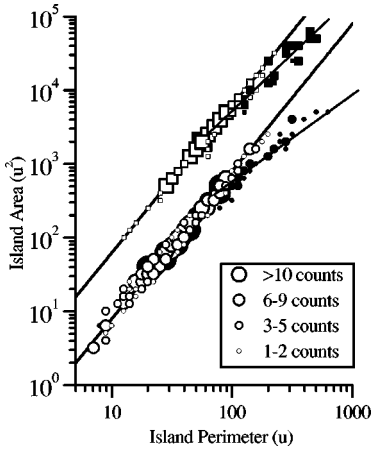

FIG. 3. Area-perimeter relation for synthetic data. The top line (square islands) has been scaled by a factor of 10 over the bottom line (round islands). A difference in the ρ value [Eq. (11)] is visible between the two lines. The size of the symbols represents the number of points clustered together. The solid points represent data for a threshold of 0.5 (runtogether allowed); the hollow 1, which only allows islands of the given shape.

$$P(\delta)=\rho\delta^{(1-D')}A(\delta)^{D'/2}. \tag{11}$$

This equation is dependent on the ''yardstick length'' δ as discussed by Mandelbrot.[1] In the case of digitized STM images, δ is the pixel size, which varies with image size.

We first demonstrate this relation by applying it to synthetic data. Images were generated which consisted of islands with a randomly generated diameter and lateral position. Each island was the same shape, with height 1. The ''coastline'' of the island had height 0.5, forming an intermediate level between ''land'' and ''sea,'' which had a height of 0. The islands were allowed (but not compelled) to touch at the ''coastline'' level, but not to overlap at the height $=1$ level. The images were then digitized to form 512×512 pixel images, which were given an arbitrary length scale of 500 units. A $2.5\times$ magnification of the original image was then made, digitized, and assigned a length of 200 units.

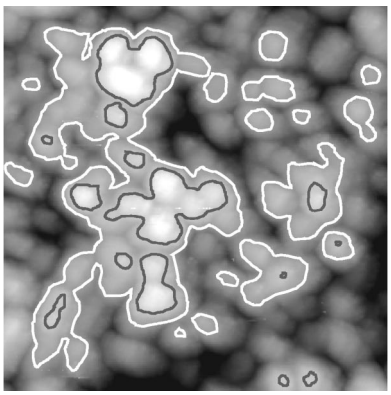

FIG. 4. STM image of 5 nm Fe grown at 295 K, with a scan length 50 nm. The shapes resulting from the highest and lowest thresholds are superposed. Islands touching the sides of the image are neglected.

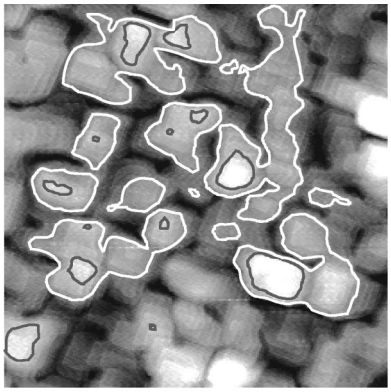

FIG. 5. STM image of 5 nm Fe grown at 595 K, with a scan length 200 nm. Contours as Fig. 4.

The sizes of the islands were then measured using commercial software. A threshold z_t is chosen; points above this level are assigned as ''land,'' the remainder as ''sea.'' An automatic algorithm then measures the area and apparent perimeter, neglecting islands that touch the sides of the image field. If z_t is chosen as 1, then only the islands themselves will be measured, since the ''coastline'' that connects chains of islands will be ignored. Setting $z_t=0.5$ allows these smaller islands to ''run together,'' forming complex shapes.

Figure 3 shows the area-perimeter relations for square and round islands. The lighter superposed lines follow the law given in Eq. (7). For $z_t=1$ (open points), no deviation from this law is found — the surface is nonfractal. When $z_t=0$ (filled points), points falling away from this law above 100 units perimeter were seen. These chains of islands give D' values of 1.7 ± 0.05 (circles) and 1.3 ± 0.3 (squares). The rescaling of the image to differing resolutions affects δ, but in this region the behavior is nonfractal, so A/P is constant. In any case, changes to δ do not affect the power-law relation between A and P. The expected change in ρ between circular and square islands is also found.

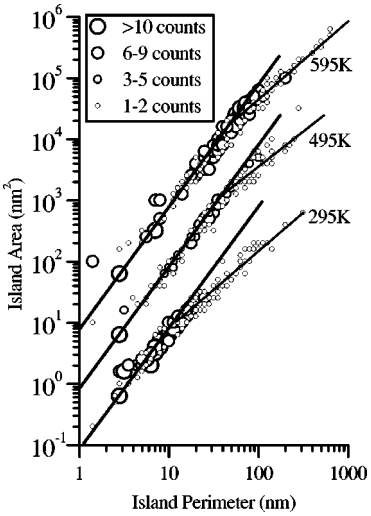

FIG. 6. Area-perimeter relation for STM images. Top 595 K growth temperature, middle, 495 K, bottom, 295 K. The sizes of the circles reflect the number of points clustered together. The variation in average island size can clearly be seen. The top two data sets have been scaled by factors of 10 to separate the curves.

TABLE II. Data from the area-perimeter measurements (see Sec. IV). The fractal dimension (D') is given, as is the point at which the line fitting fractal behavior meets the line $D'=1$.

Growth temp. (K)	D'	Perimeter intercept P_c (nm)	Radius intercept (nm)	Mean-island area [$(nm)^2$]	Area s.d. [$(nm)^2$]
295	1.58 ± 0.03	13	2	13	27
495	1.77 ± 0.06	39	6	42	43
595	1.82 ± 0.02	76	12	80	115

Selected STM images used for the roughness study were analyzed by this method. Images of various scan sizes were used, each image providing approximately 100 islands. Three different z_t values were used, providing islands ranging from pinnacles only a few pixels across to complex shapes covering a large area. Typical results of the thresholding procedure are shown in Figs. 4 and 5.

Figure 6 shows the area-perimeter relation for the STM images. The lines represent Eq. 7 for circular islands. As with the synthetic data, the smaller islands fall on the expected square law, fractal behavior being seen in the larger islands. Deviations from Eq. (7) can also be seen at smaller perimeters; this is an artifact due to the software measuring islands that consist of few pixels. Table II gives the fitted values of D', which are seen to increase with increasing deposition temperature. The perimeter at which the line representing Eq. (11) meets the squarelaw P_c is presented, as is its equivalent radius, $P_c/2\pi$. The high standard deviation from the mean-island area is accounted for by the fact that islands with an area 2 orders higher than the mean are present. For this reason, these figures are not directly comparable with those in Table I.

V. DISCUSSION

The results of Sec. III should be compared with previous reports[14,18,28] in which multiple image variography (MIV) is used to assess length-dependent roughness. MIV is the measurement of roughness over various sized sections of images, and yields curves similar in appearance to Fig. 2. The parameter ''rms roughness'' $\sigma(L)$ is in fact a measure of the deviation of the surface from the mean height. As smaller and smaller sections of the surface are examined, the mean heights for each section will begin to differ from the mean height of the overall image. Thus, the mean becomes closer to the average height of the section, and $\sigma(L)$ becomes smaller.

MIV is also generally used to average over square sections of images, so to compare with direct evaluation of Eq. (1) we must consider the fact that MIV averages over all the lengths present in the square. We can derive the exact relation between $g(L)$ and the more commonly reported $\sigma(L)$ using the distribution of lengths within a discrete unit square, $\rho_d(l)$.[29]

We can now write the relation using $\rho_d(l)$ as a weighting function:

$$\sigma(L)=\int_0^\infty \rho_d(l/L)g(l)dl. \tag{12}$$

Phenomenologically, both $g(L)$ and $\sigma(L)$ yield the same σ_∞ and approximately the same H:

$$\sigma(L)\approx aL^{2H}\int_0^\infty \sigma(l)l^{2H}dl \quad \text{for} \quad l\gg\xi. \tag{13}$$

However, ξ is shifted in the positive x direction with respect to $g(L)$ (in the case of a log-log plot).

We were able to show that our images were correctly plane-fitted, since $g(L)$ had truly saturated. However, plane-fitting must be used with discretion, since its use on images of side smaller than ξ will result in corruption of the image and give incorrect values for $g(L)$. The height-height variance function allows us not only to measure σ_∞, but to assess its validity since artifacts such as tip collisions and dirt particles prevent $g(L)$ from saturating.

We conclude that Eq. (1) gives more meaningful results than the MIV since $\sigma(L)$ yields only approximate values of H and ξ. However, MIV requires slightly less computational effort. The correct values for D allowed us to resolve a clear increase in the fractal dimension at the highest temperature, which could not be resolved using variography.[28] This change supported the report of Thürmer *et al.*[7] that different film morphology results at temperatures above 500 K due to atoms being able to diffuse downwards at step edges. The values for ξ are numerically close to the average island radii. We attribute the difference at 295 K to the fact that there is a wider variation in island heights at this temperature, increasing ξ.

The thresholding procedure used prior to the area-perimeter analysis reduces the three-dimensional STM image to a two-dimensional set of points. This results in a dimension D' between 1 and 2, which is not directly comparable to D. There is evidence for an increase in D' with temperature. The parameter $P_c/2\pi$ is consistently smaller than the mean-island radius.

ACKNOWLEDGMENTS

This work has been financially supported by the Dutch Foundation for the Fundamental Research of Matter, which is, in turn, financially supported by the Dutch Organization for Scientific Research. R.S. would like to acknowledge the assistance of the Brite-Euram program of the European Community (Contract No. BRE 2-CT93-0569). D.J.L.H. would like to acknowledge the support of the Studienstiftung des Deutschen Volkes.

*Author to whom correspondence should be addressed. Fax: +31243652190. Electronic address: hvk@sci.kun.nl

[1] B. B. Mandelbrot, *The Fractal Geometry of Nature* (Freeman, New York, 1983).
[2] J. Villain, J. Phys. I **19**, 1 (1991).
[3] M. Siegert and M. Plischke, Phys. Rev. Lett. **73**, 1517 (1994).
[4] M. Siegert and M. Plischke, Phys. Rev. E **50**, 917 (1994).
[5] I. Heyvaert, J. Krim, C. van Haesendonck, and Y. Bruynseraede, Phys. Rev. E **54**, 349 (1996).
[6] G. Dumpich and S. Friedrichowski, Thin Solid Films **260**, 239 (1995).
[7] K. Thürmer, R. Koch, M. Weber, and K. H. Rieder, Phys. Rev. Lett. **75**, 1767 (1995).
[8] G. Palasantzas and J. Krim, Phys. Rev. Lett. **73**, 3564 (1994).
[9] K. Temst, M. J. van Bael, B. Wuyts, C. van Haesendonck, Y. Bruynseraede, D. G. de Groot, N. Koeman, and R. Griessen, Appl. Phys. Lett. **67**, 3429 (1995).
[10] J. M. Gómez-Rodríguez, A. Asenjo, R. C. Salvezza, and A. M. Baró, Ultramicroscopy **42-44**, 1321 (1992).
[11] J. Barnás and Y. Bruynseraede, Phys. Rev. B **53**, 5449 (1996).
[12] E. E. Fullerton, D. M. Kelly, J. Guimpel, I. K. Schuller, and Y. Bruynseraede, Phys. Rev. Lett. **68**, 859 (1992).
[13] R. Schad, D. Bahr, J. Falta, P. Beliën, and Y. Bruynseraede, J. Phys.: Condens. Matter **10**, 61 (1998).
[14] M. H. V. Rao, B. K. Mathur, and K. L. Chopra, Appl. Phys. Lett. **65**, 124 (1994).
[15] A. Kaserer and E. Gerlach, Z. Phys. B **97**, 139 (1995).
[16] E. Z. Luo, S. Heun, M. Kennedy, J. Wollschläger, and M. Henzler, Phys. Rev. B **49**, 4858 (1994).
[17] R. C. Salvarezza, L. Vázquez, P. Herrasti, P. Ocón, J. M. Vara, and A. J. Arvia, Europhys. Lett. **20**, 727 (1992).
[18] J. D. Kiely and D. A. Bonnell, J. Vac. Sci. Technol. B **15**, 1483 (1997).
[19] J. M. Williams and T. P. Beebe, J. Phys. Chem. **97**, 6249 (1993).
[20] N. Almqvist, Surf. Sci. **355**, 221 (1996).
[21] S. M. Jordan, J. F. Lawler, R. Schad, and H. van Kempen, J. Appl. Phys. **84**, 1499 (1988).
[22] S. K. Sinha, E. B. Sirota, S. Garoff, and H. B. Stanley, Phys. Rev. B **38**, 2297 (1988).
[23] J. Feder, *Fractals, Physics of Solids and Liquids* (Plenum, New York, 1988).
[24] R. L. Schwoebel, J. Appl. Phys. **40**, 614 (1969).
[25] J. Krim, I. Heyvaert, C. Van Haesendonk, and Y. Bruynseraede, Phys. Rev. Lett. **70**, 57 (1993).
[26] J. Villarrubia, Surf. Sci. **321**, 287 (1994).
[27] G. Reiss, J. Vancea, H. Wittmann, J. Zweck, and H. Hoffmann, J. Appl. Phys. **67**, 1156 (1990).
[28] S. M. Jordan, R. Schad, J. F. Lawler, D. J. L. Herrmann, and H. Van Kempen, J. Phys.: Condens. Matter **10**, L355 (1998).
[29] The distribution of lengths within a unit continuous square, $\rho(L)$ is given by

$$\rho(l)=\begin{cases} 2l(\pi-4l+l^2) \quad \text{for } 0\leqslant l\leqslant 1 \\ \displaystyle\int_{\sqrt{l^2-1}}^{1}\int_{0}^{1-\sqrt{l^2+a^2}} l \\ \times[\,\pi/2-\cos^{-1}(a/l)-\cos^{-1}\{(1-b)/l\}]\,dbda \\ \text{for } 1<l\leqslant\sqrt{2} \\ 0 \quad \text{for } l>\sqrt{2} \end{cases} \tag{14}$$

This relation is only strictly true when l can vary continuously; however for a 256 square grid an error of only 10% is incurred.